Comparison of the $U_{37}^{K'}$, LDI, TEX_{86}^{H} and RI-OH temperature proxies in the northern shelf of the South China Sea

Bingbing Wei[1, 2], Guodong Jia[1], Jens Hefter[2], Manyu Kang[1], Eunmi Park[2, 3, 4] and Gesine Mollenhauer [2, 3, 4]

[1]State Key Laboratory of Marine Geology, Tongji University, Shanghai, 200092, China
[2]Alfred Wegener Institute, Helmholtz Center for Polar and Marine Sciences, Bremerhaven, 27570, Germany
[3]Department of Geosciences, University of Bremen, Bremen, 28359, Germany
[4]MARUM, Center for Marine Environmental Sciences, University of Bremen, Bremen, 28359, Germany

Correspondence to: Guodong Jia (jiagd@tongji.edu.cn), Gesine Mollenhauer (gesine.mollenhauer@awi.de)

Abstract. The temperature proxies $U_{37}^{K'}$, LDI, TEX_{86}^{H} and RI-OH are derived from lipid biomarkers, namely long-chain alkenones from coccolithophorids, archaeal glycerol dialkyl glycerol tetraethers (GDGTs), long-chain diols ascribed tentatively to eustigmatophytes, and archaeal OH-GDGTs, respectively. The applicability of these proxies has been examined in the South China Sea (SCS), but most of these studies were focused on a single proxy and hence did not allow for a direct comparison between them. In this study, we investigated the above 4 proxies in the same set of surface sediment samples in the northern SCS shelf and related them to local sea surface temperature (SST), which allowed us to assess whether they represent certain seasons or are impaired by terrestrial influences, as well as to infer the preferred habitats of their source organisms. Terrestrial organic inputs appeared to have an impact on LDI, TEX_{86}^{H} and RI-OH proxies near the coast and lead to colder LDI and TEX_{86}^{H} derived temperatures, but a warmer RI-OH estimate in this region. After excluding samples influenced by terrestrial organic input, we found that LDI-derived temperature agreed well with annual SSTs, while $U_{37}^{K'}$ reflected mainly spring SST and both TEX_{86}^{H} and RI-OH indices were correlated with winter SST. The differential seasonal biases of these biomarker-derived temperatures observed here suggest that each biomarker's source organism responds differently to regional marine environmental changes in an annual cycle. Specifically, marine eustigmatophytes are likely insensitive to nutrient variations and hence show the lowest seasonal variations, while coccolithophorids could have bloomed in late spring, when nutrient inputs by freshwater are usually highest. GDGT- and OH-GDGT-producing planktonic archaea likely thrive in winter, when conditions, such as relatively high nutrients levels, low light, and high concentrations of SPM in the upper water due to the enhancement of vertical mixing driven by a combination of surface cooling and strong winter monsoon winds, are favorable, although not clearly known.

1 Introduction

30 Over the past three decades, organic proxies have been successfully applied to reconstruct the Quaternary or even Cenozoic temperature history of the Earth's surface ocean. The two most widely used proxies are the $U_{37}^{K'}$ from alkenones (Brassell et al., 1986) and the TEX$_{86}$ based on archaeal isoprenoid tetraethers (Schouten et al., 2002). More recently, two additional organic thermometers, the LDI (long chain diol index) and RI-OH (ring index of hydroxylated isoprenoid glycerol dialkyl glycerol tetraethers (OH-GDGTs)), have been proposed by Rampen et al. (2007) and Lü et al. (2015).

35 The $U_{37}^{K'}$ proxy is based on the unsaturation of C_{37}-alkenones that were synthesized by a very restricted group of haptophyte algae, most notably the coccolithophores *Emiliania huxleyi* and *Gephyrocapsa oceanica* in typical marine environments (Farrimond et al., 1986; Volkman and L, 1995). Haptophyte algae are light-dependent and live near the sea surface with a competitive advantage in phosphorous-limited environments (Müller et al., 1998; Paasche, 2002). The TEX$_{86}$, as well as its modified versions TEX$_{86}^{H}$ and TEX$_{86}^{L}$, is based on the relative abundance of isoprenoid glycerol dialkyl glycerol tetraethers

40 (iGDGTs) containing 0–3 cyclopentane moieties (GDGT-0, 1, 2, 3, respectively) or an additional cyclohexane moiety (crenarchaeol and its regio isomer), produced by marine planktonic Thaumarchaeota (Schouten et al., 2013). Thaumarchaeota play an important role in pelagic ammonia oxidation in marine environments, and tend to maximize in abundance at subsurface depths <200 m (Schouten et al., 2013). The LDI index is derived from the long-chain diols (LCDs), the producers of which, albeit not unambiguously identified yet, likely are eustigmatophyte algae in marine environments

45 (Rampen et al., 2007, 2014a). Similarly, little is known about the biological sources of OH-GDGTs and their influence on the RI-OH proxy. Culture studies suggest that Thaumarchaeota Group 1.1a (e.g., *Nitrosopumilus maritimus*) and a strain of thermophilic euryarchaeota *Methanothermococcus thermolithotrophicus* could synthesize OH-GDGTs (Liu et al., 2012b; Sinninghe Damsté et al., 2012).

Due to the distinctive ecology of their source organisms, these temperature proxies differ in reflecting water temperatures in

50 terms of, e.g., water depth and seasonality. For instance, in the South China Sea (SCS), the $U_{37}^{K'}$ and TEX$_{86}^{H}$ indices likely reflect temperatures of the mixed layer (>30 m) and the subsurface (30–125 m), respectively (Jia et al., 2012). However, in the shallow coastal area of the SCS, the $U_{37}^{K'}$-derived SST estimates are biased toward the spring and summer temperatures, but those based on TEX$_{86}^{H}$ toward the winter temperature, likely due to different blooming times (Zhang et al., 2013). By contrast, in the East China Sea (ECS), both TEX$_{86}^{H}$ and RI-OH signals are summer biased (Lü et al., 2014, 2019; Zhang et al.,

55 2017). Lopes et al. (2013) compared the $U_{37}^{K'}$, TEX$_{86}^{H}$ and LDI indices in sediments from offshore southeastern Australia, and found that LDI-derived temperature compares well with the temperatures of the warmest month, TEX$_{86}^{H}$ with the temperatures of the coolest month and $U_{37}^{K'}$ with mean annual temperature. While in the southeast Australian ocean, $U_{37}^{K'}$ and LDI provide better estimates of winter temperature at the surface, and TEX$_{86}^{H}$ matches well with annual temperature within 75–100 m (Smith et al., 2013).

60 The accuracy of organic thermometers is also prone to be impaired by a low specificity of related biomarkers. For example, the noncalcifying haptophyte genera *Isochrysis galbana* and *Chrysotila lamellose*, are predominantly restricted to non-

marine and marginal settings and expected to produce distinctly different alkenone records, which are likely to "contaminate" the $U^{K'}_{37}$ signal in marginal seas (Bijma et al., 2001). GDGTs synthesized by soil archaea and marine Euryarchaeota are likely different in composition from those produced by marine Thaumarchaeota, which could introduce biases to TEX_{86} values in

65 conditions with inputs of archaeal lipids from multiple sources (Schouten et al., 2013; Turich et al., 2007; Weijers et al., 2006). Recently, the LDI proxy was found to be limited by the input of 1,13 and 1,15-diols from fresh-water eustigmatophyte algae, especially in the coastal seas (Balzano et al., 2018; de Bar et al., 2016). Similarly, OH-GDGTs may occur also in terrestrial environments including rivers (Chen et al., 2016; Kang et al., 2017), lakes (Liu et al., 2012a) and soils (Kang et al., 2017), which could also bias the RI-OH index in marginal seas.

70 Coastal seas are an ideal place for evaluation of the influences on the organic temperature proxies of various confounding factors, due to its environmental and ecological seasonality and transition from the land to the deep-sea. In this study, we analysed alkenones, LCDs and GDGTs in surface sediments from the northern SCS shelf. $U^{K'}_{37}$, TEX^{H}_{86}, LDI and RI-OH indices have been studied in this area (Chen et al., 2018; Ge et al., 2013; Jia et al., 2017, 2012b; Wei et al., 2011; Zhang et al., 2013; Zhu et al., 2018), however most of these studies were focused on a single proxy and hence lacked a direct comparison

75 between them. Here, we investigated all of the above 4 temperature proxies in the same surface sediment samples and evaluated their applicability as water temperature indicators. This effort would benefit regional multi-proxy sea temperature reconstructions, which could be more comprehensive and objective than those based on any single ones (Eglinton and Eglinton, 2008). In addition, such kind of investigation can shed light on the ecology of the related biomarker producers in this region, which is not entirely understood at present.

2 Material and methods

2.1 Study area and sample collection

The Pearl River estuary (PRE) and the northern shelf of SCS lie in a (sub)tropical monsoon climate region, with strong northeast winds in winter and weaker southwest winds in summer (Liu and Xie, 1999). As a result, coastal currents flow southwestward in winter (Fig. 1b), causing a strong vertical mixing and an inshore-offshore temperature gradient, while in

85 summer, coastal currents reverse direction, except for one, which was near the western coast of the Pearl River (PR) and flow southwestward due to the large outflow of the PR (Fig. 1c, Liu and Xie, 1999; Su, 2004).

In the study area, a total of 23 core-top sediments (0–1 or 0–2 cm depths) were collected from the PRE and the coastal northern SCS, from water depths ranging from 6.5 to 1307 m (Suppl. Table 1). The samples were collected using a gravity box corer or grab sampler and then frozen at −20 °C in the laboratory before treatment.

2.2 Lipid extraction and separation

After being freeze-dried and homogenized, about 5 g of sediments were ultrasonically extracted three times with DCM: MeOH (9:1, v/v) for 15 min. Before extraction, known amounts of 2-nonadecanone, androstanol and C_{46} GDGT were added as internal standards. Supernatants of each extraction were obtained by centrifugation. The total lipid extracts were combined and concentrated with rotary evaporation to ~1 mL, and saponified for 2 h at 80 °C with 1 mL of KOH (0.1 M) in MeOH: H_2O (9:1, v/v). The neutral fractions were extracted with *n*-hexane, and were further separated into alkane, alkenone and alcohol sub-fractions (containing diols and GDGTs) by column chromatography on silica gel using *n*-hexane, DCM: *n*-hexane (2:1, v/v) and DCM: MeOH (1:1, v/v), respectively.

2.3 Alkenone analysis and $U_{37}^{K'}$ index

Alkenones were analysed using a 7890A gas chromatograph (GC, Agilent Technologies) equipped with a cold on-column injection system, a DB-5MS fused silica capillary column (60 m, ID 250 µm, 0.25 µm film coupled to a 5 m, ID 530 µm deactivated fused silica precolumn) and a flame ionization detector (FID). Helium was used as carrier gas (constant flow, 1.5 mL/min) and the GC oven was heated using the following temperature program: 60 °C for 1 min, 20 °C/min to 150 °C, 6 °C/min to 320 °C and a final hold time of 35 min. Di-unsaturated ($C_{37:2}$) and tri-unsaturated ($C_{37:3}$) alkenones were identified by comparison of the retention times with a reference sample composed of known compounds. Peak areas were determined by integrating the respective peaks, and concentrations were calculated using the response factor of the internal standard 2-nonadecanone.

The $U_{37}^{K'}$ index was calculated using Eq. (1) after Prahl and Wakeham (1987).

$$U_{37}^{K'} = \frac{C_{37:2}}{C_{37:2} + C_{37:3}} \tag{1}$$

SST was estimated using Eq. (2) from Conte et al., (2006):

$$SST\ (°C) = \frac{U_{37}^{K'} - 0.0709}{0.0322} \tag{2}$$

2.4 Long chain diol analysis

One half of each alcohol fraction was silylated with N, O-bis(trimethylsilyl)-trifluoroacetamide (BSTFA)/1% trimethylchlorosilane (TMCS) and acetonitrile (30 µL each) and heated at 60 °C for 1 h. Diols were analysed by gas chromatography-mass spectrometry (GC/MS) on an Agilent 6850 GC coupled to an Agilent 5975C MSD operating in electron impact (EI) mode with an ionization energy of 70 eV. The GC was equipped with a fused silica capillary column (Restek Rxi-1ms, length 30 m; 250 µm ID, film thickness 0.25 µm). Helium was used as carrier gas at a constant flow rate of 1.2 mL/min. Samples (1 µL) were injected in splitless mode in a split/splitless injector (S/SL) held at 280 °C. The GC temperature program was as follows: 60 °C start temperature, held for 3 min, increased to 150 °C at a rate of 20 °C/min,

increased further to 320 °C at a rate of 4 °C/min and finally held at 320 °C for 15 min. The source temperature of the MS
120   was set to 230 °C and the quadrupole to 150 °C.

For identification of the diols, the MS was operated in single-ion monitoring (SIM) mode with the following m/z: 313.3 (C_{28}
1,13-diol, C_{30} 1,15-diol), and 341.3 (C_{30} 1,13-diol, C_{32} 1,15-diol) (Versteegh et al., 1997; Rampen et al., 2012). Fractional
abundances of the long chain diols were calculated from integrated relevant peak areas in respective mass chromatograms.
The LDI was calculated and converted to SST using Eq. (3) and Eq. (4) from Rampen et al. (2012):

125    $$LDI = \frac{[C_{30}\ 1,15]}{[C_{28}\ 1,13] + [C_{30}\ 1,13] + [C_{30}\ 1,15]}$$ (3)

$$SST\ (°C) = \frac{LDI - 0.095}{0.033}$$ (4)

The %C_{32} 1,15 index reflecting riverine input was calculated using Eq. (5) given by Lattaud et al. (2017) as follows:

$$\%C_{32}\ 1,15 = \frac{[C_{32}\ 1,15]}{[C_{32}\ 1,15] + [C_{30}\ 1,15] + [C_{28}\ 1,13] + [C_{30}\ 1,13]} \times 100$$ (5)

2.5 GDGT analysis and indices (TEX$_{86}^{H}$, BIT, MI, and RI-OH)

130   GDGTs were analysed by high performance liquid chromatography (HPLC) coupled via an atmospheric pressure chemical
ionization (APCI) interface to a single quadrupole mass spectrometer (MS), with a method slightly modified from Hopmans
et al. (2016). Analyses were performed on an Agilent 1200 series HPLC system and an Agilent 6120 MSD. Separation of the
individual GDGTs including the 5-/6-methyl isomers of branched-GDGTs was achieved on two UPLC silica columns in
series (Waters Acquity BEH HILIC, 2.1×150 mm, 1.7 µm), with a 2.1×5 mm pre-column of the same material maintained at
135   30 °C. Mobile phase A and B consisted of *n*-hexane: chloroform (99:1, v/v) and *n*-hexane: 2-propanol: chloroform (89:10:1,
v/v/v), respectively. After sample injection (20 µL) and 25 min isocratic elution with 18 % mobile phase B, the proportion of
B was linearly increased to 50 % within 25 min, and thereafter to 100 % for the next 30 min. After another 5 min and prior to
the analysis of the next sample, the column was re-equilibrated with 18 % B for 15 min. The flow rate was 0.22 mL/min and
a maximum back pressure of 220 bar was obtained. The total run time was 100 min.
140   GDGTs were detected using positive ion APCI-MS and selective ion monitoring (SIM) of their (M+H)$^{+}$ ions (Schouten et al.,
2007) or abundant ion-source fragmentation products of OH-GDGTs (Liu et al., 2012). APCI spray-chamber conditions
were as follows: nebulizer pressure 50 psi, vaporizer temperature 350 °C, N_2 drying gas flow 5 L/min and 350 °C, capillary
voltage (ion transfer tube) −4 kV and corona current +5 µA. The MS-detector was set for SIM of the following (M+H)$^{+}$ ions:
m/z 1302.3 (GDGT-0), 1300.3 (GDGT-1+OH-GDGT 0), 1298.3 (GDGT-2+OH-GDGT-1), 1296.3 (GDGT-3+OH-GDGT-2),
145   1292.3 (GDGT-4+4′/Crenarch-aeol+regio-isomer), 1050 (GDGT-IIIa/IIIa'), 1048 (GDGT-IIIb/IIIb'), 1046 (GDGT-
IIIc/IIIc'), 1036 (GDGT-IIa/IIa'), 1034 (GDGT-IIb/IIb'), 1032 (GDGT-IIc/IIc'), 1022 (GDGT-Ia), 1020 (GDGT-Ib), 1018
(GDGT-Ic) and 744 (C_{46} standard), with a dwell time of 57 ms per ion.

Quantification of the individual GDGTs was achieved by integrating the respective peak areas. Compound contents were calculated using the response factor obtained from the C_{46} standard and by normalizing to the amount of extracted sediment.

150 Due to the lack of appropriate standards, individual relative response factors between the C_{46} standard and the different GDGTs could not be considered, the obtained concentrations should therefore be regarded as being only semi-quantitative.

The TEX_{86} and TEX_{86}^H were calculated following Eq. (6) and Eq. (7) and converted to SST according to Eq. (8) given by Kim et al. (2010), which is suitable to reconstruct SST between 15 and 30 °C.

$$TEX_{86} = \frac{GDGT\text{-}2 + GDGT\text{-}3 + Cren'}{GDGT\text{-}1 + GDGT\text{-}2 + GDGT\text{-}3 + Cren'} \tag{6}$$

155 $$TEX_{86}^H = \log(TEX_{86}) \tag{7}$$

$$SST\ (°C) = 68.4 \times TEX_{86}^H + 38.6 \tag{8}$$

The BIT index was calculated according to Hopmans et al. (2004) including 6-methyl brGDGTs (DeJonge et al., 2013):

$$BIT = \frac{Ia + IIa + IIIa + IIa' + IIIa'}{Ia + IIa + IIIa + IIa' + IIIa' + Cren} \tag{9}$$

where Ia is the basic tetramethyl brGDGT; IIa and IIIa are 5-methyl brGDGTs; IIa' and IIIa' are 6-methyl brGDGTs

160 (DeJonge et al., 2013).

The methane index (MI) was calculated using the Eq. (10) given by Zhang et al. (2011):

$$MI = \frac{GDGT\text{-}1 + GDGT\text{-}2 + GDGT\text{-}3}{GDGT\text{-}1 + GDGT\text{-}2 + GDGT\text{-}3 + Cren + Cren'} \tag{10}$$

The RI-OH index was calculated using Eq. (11), and converted to annual mean SST according to Eq. (12) (Lü et al., 2015):

$$RI\text{-}OH = \frac{[OH\text{-}GDGT\text{-}1] + 2 \times [OH\text{-}GDGT\text{-}2]}{[OH\text{-}GDGT\text{-}1] + [OH\text{-}GDGT\text{-}2]} \tag{11}$$

165 $$SST\ (°C) = \frac{RI\text{-}OH - 0.92}{0.028} \tag{12}$$

2.6 Climatological mean temperature data

Annual and seasonal SST data for each sampling site were 8–years average values (2005–2012) taken from the NOAA World Ocean Atlas 2013 (WOA13 V2) on a 0.25° grid resolution (https://www.nodc.noaa.gov/cgi-bin/OC5/woa13/woa13.pl), which is the latest version and close to the estimated deposition time ([sampling time, 2012–

170 2017)] – [depth, 0–2 cm))/[deposition rate, 2-6 mm yr^{-1}] = [deposition time, 2002-2014)) (Ge et al., 2014; Liu et al., 2014). According to the description of WOA13, seasons were defined as follows: Winter: January–March; Spring: April–June; Summer: July–August; Autumn: September–December. In addition, the residual of a proxy-derived SST relative to the WOA13 SST was calculated as follows:

Residual (°C) = [proxy-derived temperature] – [WOA13-derived temperature] $\tag{13}$

3 Results

3.1 Hydrological parameters

Except one sample taken from deeper waters (LD-21, WD = 1307 m), the sites of surface sediment samples in this study were mainly located on the shelf area (WD <200 m) (Fig. 1a). The measured annual mean SSTs (0 m depth, from the WOA13 dataset) in the study area ranged between 24.2 °C and 26.8 °C (25.5 °C average), and showed clear seasonal variations exhibiting low values in winter (21.2 °C average), highest in summer (29.0 °C average), and intermediate in spring (26.3 °C average) and autumn (25.6 °C average) (Fig. 2). The temperatures of the mixed layer (0–30 m) were slightly (<0.8 °C) lower than SST and also varied seasonally in a similar pattern (Suppl. Table 1). The annual mean and seasonal SSTs displayed an increasing trend offshore with the largest difference of ca. 6 °C in winter between inshore and offshore.

3.2 $U_{37}^{K'}$ and alkenone-derived temperatures

The $U_{37}^{K'}$ index ranged between 0.81 and 0.94 (0.91 average) (Suppl. Table 2), corresponding to 23.0–27.0 °C (26.0 °C average, Fig. 2) based on the calibration proposed by Conte et al. (2006). Compared with the measured SSTs, the $U_{37}^{K'}$-SSTs were closest to the spring SST at most sites, except two inshore samples (WD <50 m), which had slightly lower $U_{37}^{K'}$-SSTs (Fig. 2). We also compared results from different calibrations for 0 m or 0–30 m SSTs (Suppl. Fig. 1), and found that all derived $U_{37}^{K'}$-SSTs exhibited similar values that differed from the calibration of Conte et al. (2006) by <0.7 °C (0.1 °C average; Suppl. Table 2). For this study, we considered only the temperatures calculated by Conte et al. (2006).

3.3 LCD distribution and LDI-derived temperatures

In the total 1,13- and 1,15-diols, the C_{30} 1,15-diol was the most abundant (>80 %) at most sites outside the PRE, followed by C_{32} 1,15-diols (<15 %) and C_{28} and C_{30} 1,13-diols (<4 %) (Fig. 3). However, the C_{32} 1,15-diols were more abundant (>41 %) than the C_{30} 1,15-diols (>19 %) in the PRE sediments. The C_{28} and C_{30} 1,13-diols exhibited a similar spatial distribution pattern as the C_{32} 1,15-diol, showing higher relative abundances in the PRE and coastal area (Fig. 3).

The LDI values of surface sediments varied from 0.56 to 0.98, but were ≥0.90 at most sites, corresponding to LDI-derived temperatures (LDI-SST) varying from 14.0 to 26.9 °C (Fig. 2). The river input index (%C_{32} 1,15) values ranged from 1.9 % to 66.3 %, showing an overall decreasing trend offshore (Suppl. Table 3-1). A comparison of our LDI values and the global data from Rampen et al. (2012) indicated that our data agreed well with the global data, except for three samples with low LDI values and hence resulting in substantial annual SST residuals (<−7 °C) (Suppl. Fig. 2). Two of the three samples were located in the PRE and the other one in the inshore area (Site MMDB, WD = 26 m). In addition, we also found that the third PRE sample at PRE-Y11 as well as samples GLB and SXCB near the coast (WD = 15 m and 14 m, respectively) exhibited significant annual SST residuals (<−2.1 °C). When excluding data from these six samples, our LDI-SSTs were close to annual SSTs, with residuals ranging between −0.3 °C and 1.2 °C (Suppl. Table 3-1 and 3-2).

3.4 Distribution of GDGTs, TEX$_{86}^{H}$ and RI-OH-derived temperatures

The iGDGTs were dominated by crenarchaeol ([Cren], 43.2–65.9 %) and GDGT-0 ([0], 18.1–37.0 %) (Fig. 4a), and the ratios of both compounds, i.e. [0]/[Cren], ranged between 0.28 and 0.75 (Fig. 4c). Two samples with relatively high values of [0]/[Cren] were from the PRE (0.75, PRE-A8) and the deep sea (0.69, LD-21) (Fig. 4c). The least abundant iGDGTs is the crenarchaeol regio isomer ([Cren'], 0.8–5.4 %), showing an overall increasing trend offshore (Fig. 4a). The ratio of GDGT-0 and crenarchaeol regio isomer, i.e. [0]/[Cren'], maximized in the river mouth (47.3, PRE-A8) and exhibited a declining trend offshore (Fig. 4d). The ratio of GDGT-2 versus GDGT-3, i.e. [2]/[3], ranged from 2.6 to 7.2, and was low at shelf and coastal sites (WD <200 m, 2.6–3.6), but high at the deep-sea site (7.2, LD-21) (Fig. 4d). Similar spatial distribution patterns appeared also for the [2]/[Cren] ratio and the MI value, exhibiting low values of 0.07–0.15 for [2]/[Cren] and 0.16–0.26 for MI at shelf and coastal sites, and slightly higher values of 0.25 for [2]/[Cren] and 0.31 for MI at the deep-sea site (LD-21) (Fig. 4c). In addition, higher BIT values (0.49) were found in the PRE, relative to the inshore area (0.1–0.3, WD <50 m) and the offshore area (<0.1) (Fig. 4c).

The OH-GDGTs contributed 1.5–4.1% to the total GDGT pool (Suppl. Table 5), consistent with the lower relative OH-GDGTs abundance found in (sub)tropical regions (Huguet et al., 2013). The most abundant OH-GDGT is OH-GDGT-2 ([OH-2], 39.2–67.0 %), with high values at shelf and coastal sites (WD ≤186 m) (Fig. 4b), but low contribution at the deep-sea site (LD-21). In contrast, the relative abundance of OH-GDGT-0 ([OH-0]) remained low at shelf and coastal sites, but was elevated at the deep-sea site (Fig. 4b). In addition to the twenty sediment samples used in this study, there have been 47 other reported data of OH-GDGTs in the surface sediments in the SCS from water depths ranging between 3 m and 4405 m (Lü et al., 2015; Yang et al., 2018). By combining these data, we observed a positive logarithmic correlation between [OH-0] and water depth (R^2 = 0.58), but a negative logarithmic correlation between [OH-2] and water depth (R^2 = 0.66) (Fig. 4b).

TEX$_{86}^{H}$ values varied in the range between −0.33 and −0.18 (Suppl. Table 4), corresponding to SST values of 16.2 to 26.0 °C based on the calibration by Kim et al. (2010). The annual residuals ranged from −8.8 to −0.8 °C. Seasonally, the mean absolute values of residuals were 2.0 °C, 6.0 °C, 8.7 °C and 5.3 °C, respectively, from winter to autumn (Suppl. Table 4), indicating TEX$_{86}^{H}$-SSTs were closer to winter temperature. Spatially, consistently low temperature estimates were found in the coastal area and PRE with water depth <50 m, some of them even colder than winter SST (Fig. 2). However, the offshore samples had relatively high TEX$_{86}^{H}$-SSTs, which were ca. 2 °C higher than winter SST and close to autumn and annual SSTs (Fig. 2).

The RI-OH values varied from 1.57 to 1.79 (Suppl. Table 5), which agree with recently reported data for the same region (1.50–1.75) (Lü et al., 2015; Yang et al., 2018). SST estimates based on the calibration suggested by Lü et al. (2015) for the Chinese marginal sea (CMS), were within a range of 23.3–31.2 °C (Fig. 2). In comparison with the measured annual SST, three higher RI-OH-SSTs occurred in the PRE, with annual residuals of 2.6–6.2 °C, and other samples exhibited slightly higher or lower RI-OH-SSTs, with annual residuals of −2.5–3.1 °C (Fig. 2 and Suppl. Table 5).

4 Discussion

4.1 Seasonality of the $U_{37}^{K'}$ proxy

Although the relationship between $U_{37}^{K'}$ and SST is robust and well supported by culture studies, the seasonality of production
240 of C_{37} alkenones and the response of $U_{37}^{K'}$ to temperature at very warm and cold environments remain unresolved (Tierney and Tingley, 2018). Sediment trap studies demonstrated that alkenone production varies markedly across the oceans, with factors such as temperature, nutrients, light availability, and competition regulating the timing of haptophyte blooms (Rosell-Melé and Prahl, 2013). The seasonality of alkenone production may be transferred to sediments, but this signal could also be altered by the complex sedimentation processes (Rosell-Melé and Prahl, 2013). Our results indicated that $U_{37}^{K'}$-SST estimates
245 were spring biased in this region (Fig. 2). A similar finding has been reported by Zhang et al. (2013), who proposed $U_{37}^{K'}$-SST to be summer-biased. We note that summer in that work included June, July and August, differing from the definition used here, where the month of June is part of spring. These suggest that the alkenone production is biased to late spring, when alkenone-source organisms are mostly bloomed. However, it has been reported that water-column coccolithophore abundance is highest both in winter and spring in the northern SCS (Chen et al., 2007), when higher nitrate concentrations
250 occur in the surface water and favour growth of coccolithophores, e.g., *E. huxleyi*. The difference between this study and others could relate to the influence of the Pearl River, and our study area was significantly impacted by the river runoff as well as the supply of terrestrial nutrients, which was highest in late spring (May to June) in an annual cycle (Dai et al., 2008; Lu and Gan, 2015; Zhang et al., 2013). The high river input with N:P ratios as high as ~100:1 could stimulate growth of alkenone-producing haptophytes, e.g., *E. huxleyi*, during this period (Xu et al., 2008), since *E. huxleyi* was reported to be
255 nitrate limited and have a competitive advantage over other phytoplankton when inorganic phosphate is limiting but nitrate is still abundant (Bijma et al., 2001).

Although a slightly lower $U_{37}^{K'}$-SST was observed in the river mouth, most of our samples exhibited a spring-biased $U_{37}^{K'}$-SST, possibly indicating that there was a low contribution of freshwater alkenones or they had less influence on $U_{37}^{K'}$-SST.

4.2 LCDs and LDI-derived temperatures

260 ### 4.2.1 Source of LCDs in the surface sediments

The unusually low LDI-derived SST estimates relative to the measured SSTs observed near the coast and close to the river mouth (Fig. 2) suggest that LDI may be influenced by terrestrial/freshwater sources other than marine producers. Similar findings were reported from the Iberian margin (de Bar et al., 2016), in the Gulf of Lion, the Berau Delta and the Kara Sea (Lattaud et al., 2017), suggestive of terrestrial influence on LCD compositions. Culture studies show that marine
265 eustigmatophyte algae mainly produce 1,13 and 1,15-diols (Rampen et al., 2007, 2014a; Volkman et al., 1999). In freshwater environments, eustigmatophyte algae primarily produce C_{32} 1,15-diol, especially in stagnant waters during dry seasons, when rivers have low-stands (Häggi et al., 2019; Lattaud et al., 2017; Rampen et al., 2014b). However, C_{30} 1,15-diols are

generally found to be dominant both in the marine water column and sediments and are likely produced by marine eustigmatophyte algae (Balzano et al., 2018).

270 To confirm the potential sources of different diols in our study area, we performed a Pearson Correlation Analysis (Table 1). We found that C_{28} and C_{30} 1,13-diols and C_{32} 1,15-diols were significantly correlated between each other (correlation coefficient: 0.56–0.83, P-value <0.005, Table 1), suggesting a similar source origin in this region. The co-occurrence of high abundance of above three diols in the PRE and along the coast rather than in the offshore area (Fig. 3) is consistent with the correlation analysis, and further suggests a terrestrial/freshwater source of them. In contrast, these three diols were

275 negatively correlated with C_{30} 1,15-diol (correlation coefficient from −0.68 to −0.90, P-value <0.005, Table 1), with the latter exhibiting an opposite pattern and showing an overall increasing trend towards the offshore. Such a spatial distribution pattern becomes more apparent when diol compositions in SPM and sediments are illustrated from the PRE to the offshore (Fig. 5). The negative correlation of C_{30} 1,15-diol with three other diols could be attributed to their different sources, i.e. marine vs. terrestrial, or an opposite response to ambient temperature of C_{30} 1,15-diol to C_{28} and C_{30} 1,13-diols.

280 **4.2.2 Influence of riverine LCDs**

Recently, Lattaud et al. (2017) presented evidence that LCDs delivered by rivers can substantially affect LDI-derived SSTs estimates in coastal regions close to river mouths. In our samples, the LDI-SST underestimated annual SST in the PRE and the near-coastal area with water depth <25 m (Fig. 2, up to −11.0 °C), but was similar to the measured annual SST at some inshore sites with water depth <25 m and all offshore sites (Fig. 2). The river input index (%C_{32} 1,15) was strongly

285 negatively correlated with annual residuals (R^2 = 0.95, Fig. 6), and samples, with %C_{32} 1,15 <20 %, have smaller annual residuals ranging between −0.3 °C and 1.2 °C (Fig. 6). After removal of data points (n = 6) with %C_{32} 1,15 >20%, indicating significant influence of riverine LCDs, the LDI-SST of the reduced data set had mean absolute values of annual SST residuals of 0.5 °C, nearly half of those of the full data set. This is similar to previous studies that %C_{32} 1,15 in the typical marine sediments generally did not exceed a value of 20 % (Lattaud et al., 2017), which could been proposed as a cut-off for

290 the reliable reconstruction of LDI-SST, and %C_{32} 1,15 above 20 % implies an increased contribution of riverine LCDs.

4.2.3 Seasonality of LDI index

Our results indicated that LDI-SSTs with minimal river influences may reflect annual SSTs (Fig. 2 and Suppl. Table 3-2), suggesting unbiased seasonal production of the source organisms of LDI in this study area. Similar results have been reported by Zhu et al. (2014), who found that LDI-SSTs in downcore sediments matched well with local annual SSTs in the

295 northern SCS. Rampen et al. (2007) found comparable annual flux of 1,15-diols at different stations in the Arabian Sea, and suggested that the biological producers of 1,15-diols do not require a high level of nutrients as needed by, e.g., *Proboscia* diatoms. Thus, LDI may reflect annual SST due to a lack of sensitivity of marine eustigmatophytes to nutrient variations in an annual cycle.

4.3 TEX$_{86}^{H}$ and isoprenoid GDGT-derived temperature estimates

300 **4.3.1 Sources of iGDGTs in the surface sediments**

In marine sediments, the iGDGTs composition may sometimes be impacted with or even controlled by non-thermal factors, e.g., sources of iGDGTs other than Thaumarchaeota (Zhang et al., 2016), and several indices (e.g., the MI and ratios of [2]/[Cren] and [0]/[Cren]) have been developed to assess the impact of these other sources on the iGDGTs distribution. Relatively low MI values (≤0.25) were observed at most sites here accompanied by low [2]/[Cren] ratios (0.07–0.15) and

305 [0]/[Cren] ratios (0.42–0.57) (Fig. 4c). These values may suggest little input of methane-related archaeal lipids, which are typically characterized by a high MI value (>0.3) or substantially elevated [2]/[Cren] and [0]/[Cren] ratios (Weijers et al., 2011; Zhang et al., 2016). The exception was the deep-sea sample (LD-21), which had a slightly higher MI value (0.31), higher [2]/[Cren] ratio of 0.25 and higher [0]/[Cren] ratio of 0.69, which could be associated with archaea involved in methane-cycling. The highest BIT value (0.49) and [0]/[Cren] ratio (0.75) were observed in the PRE (sample PRE-A8) (Fig.

310 4c), similar to the finding of Zhang et al. (2012) and indicating a significant input of soil-derived GDGTs, because BIT index in soils generally tends to be >0.9 (Hopmans et al., 2004) and [0]/[Cren] ratios in sediments in the lower reaches of the Pearl River and soils in its catchments are also high (2.6) (Wang et al., 2015).

Moreover, slightly different from other iGDGTs, [Cren'] increased clearly with increasing water depth, with the lowest value of 0.8 % found in the PRE (PRE-A8) and ~1.0 % close to the PRE (Fig. 4a). This pattern was unlikely caused by soil

315 iGDGTs input, as [Cren'] in the soils in the catchments of the Pearl River is ~3 % (Wang et al., 2015). Recently, [Cren'] as low as 0.2–0.7 %, with a mean of 0.4 %, was observed in the SPM of the lower Pearl River, which was attributed to the predominance of Euryarchaeota (Wang et al., 2015; Xie et al., 2014). In contrast, [Cren'] in deep-sea sediments in the SCS is also characterized by higher values >4 % (Jia et al., 2017).

Recently, several studies suggested that tetraether lipids of Thaumarchaeota dwelling in shallow waters are characterized by

320 [2]/[3] ratios <4 and [Cren'] <4 %, whereas for "deep-water" Thaumarchaeota lipids are characterized by higher values (Jia et al., 2017; Kim et al., 2015, 2016). It should be noted that it remains unclear what causes the different iGDGTs distribution between those two eco-types, and the depth boundary to separate the two, likely 200–300 m, is not exactly determined (Jia et al., 2017; Kim et al., 2015, 2016). Based on these criteria, only one sample, i.e. the deep-sea sample LD-21 with a [2]/[3] ratio of 7.2 and [Cren'] of 5.4 % (Fig. 4a, 4c), likely received significant contributions from deep Thaumarchaeota. The

325 sample at the second deepest site, i.e. E503 at 186 m, showed a [2]/[3] ratio of 3.6 and [Cren'] of 4.3 % (Fig. 4a, 4c), which suggests only a small contribution from deep Thaumarchaeota.

4.3.2 Seasonality of TEX$_{86}^{H}$ index

Based on the above discussion on iGDGTs indices, only two samples, one in the PRE (PRE-A8) and the other in the deep sea (LD-21), were markedly different from the remaining samples that appeared minimally influenced by soil/freshwater-

330   derived archaea and deep-dwelling Thaumarchaeota or methane-cycling archaea. After excluding data from these two

samples, we examined the temperature signal of the TEX_{86}^{H} index as below.

In the coastal area of northern SCS, TEX_{86}^{H}-derived SST in surface sediments and surface water SPM has been found lower

than annual SST and hence attributed to winter-biased archaeal production and associated iGDGTs burial (Ge et al., 2013;

Wei et al., 2011; Zhang et al., 2012; Zhou et al., 2014). Our TEX_{86}^{H}-SST estimates were 0.9–8.8 °C lower than annual SST,

335   similar to previous studies. However, when compared with winter SST, the residuals varied between −4.2 and 2.3 °C, still

showing some large negative residuals (Fig. 2).

We note that different from the global dataset utilized to establish the TEX_{86}^{H}-SST (i.e. Eq. (8)), which includes a large

number of deep-sea sediment samples, our data here were exclusively from shallow sediments receiving iGDGTs

predominantly from shallow dwelling Thaumarchaeota. Therefore, we surmise that the global TEX_{86}^{H}-SST calibration might

340   not be suitable for our study area, due to that the shallow and deep Thaumarchaeota exhibit slightly different tetraether

compositions. Alternatively, a local "shallow water" calibration could be more appropriate for temperature reconstruction in

this study. So a recent seasonal calibration based on winter surface water SPM in the SCS (Jia et al., 2017) was applied to

our data as a comparison. By applying the equation established from winter SPM ($SST_{winter} = 47.18 \times TEX_{86}^{H} + 34.44$, n = 45,

$R^2 = 0.6$) by these authors, we found that winter residuals were greatly reduced, ranging between –1.8 to 2.8 °C (Fig. 7a),

345   with only three samples having residuals ≥2.5 °C. Nevertheless, the correlation between TEX_{86}^{H} and SST, although better

than annual and other seasonal SSTs, was not strong ($R^2 = 0.41$, Fig. 7b). This could be due to other factors such as

production in other seasons, or seasonal and spatial community variations in surface water Euryarchaeota, which have been

proposed as a significant source of iGDGTs in oceanic settings (Jia et al., 2017; Lincoln et al., 2014; Turich et al., 2007;

Wang et al., 2015).

350   **4.4 RI-OH and RI-OH-derived temperatures**

4.4.1 Source of OH-GDGTs and their influences on RI-OH-SST estimates

A few studies have detected OH-GDGTs in marine, river, lacustrine and soil environments, indicating ubiquitous and

multiple sources of OH-GDGTs (Chen et al., 2016; Huguet et al., 2013; Kang et al., 2017; Liu et al., 2012; Park et al., 2019;

Wang et al., 2012). Kang et al. (2017) noted that OH-0 dominated in marine and estuarine environments (56±10 %), but OH-

355   2 was abundant in lake, river and soil environments, which may lead to overestimated RI-OH-SSTs in case of substantial

terrestrial input. Our results showed that RI-OH-SSTs were warm-biased in the PRE (Fig. 2), where terrestrial input is

significant.

In addition to terrestrial influence, RI-OH could respond to SST differently between shallow and deep environments. We

combined our data with the published values from surface sediments of the SCS, and found that, with the exception of one

360   sample (WD = 41 m), two clusters of samples can be separated based on [OH-0]/[OH-2] ratio, with shallow-water samples

(WD ≤186 m) <0.55 and deep-water samples (WD ≥330 m) >0.55 (Fig. 8a). The shallow-water samples had annual RI-OH-

SST residuals of −2.5 °C to 3.4 °C, but the deep-water samples had a larger range between −8.1 °C and 2.3 °C, implying a different thermal response or winter bias of deep-water RI-OH. Higher correlation ($R^2 = 0.65$) between annual residuals and annual SST were observed for deep-water samples (ca. 26–29 °C annual range) compared to those for shallow-water samples

365 (ca. 24–27.5 °C annual range, $R^2 = 0.05$) (Fig. 8b), indeed suggesting different thermal responses of distinct archaeal communities. This is supported by an observation of a "concave" relationship between the relative abundance of OH-2 and SST in SCS, which was explained as being due to the different responses of archaeal lipids to ambient temperature depending on whether SST is below or above 25 °C (Yang et al., 2018).

4.4.2 Seasonality of RI-OH-temperature relation in surface sediments

370 By excluding three samples from the PRE and one sample in the deep sea, we thought OH-GDGTs in the remaining samples could reflect SST in the shallow shelf waters (see section 4.3.1). We found that RI-OH index of the reduced data-set showed a relatively stronger correlation with the annual and winter SSTs ($R^2 = 0.39, 0.44$, respectively, Fig. 9) and poor correlations with other seasonal SST, indicating that RI-OH may reflect winter SST in the coastal SCS. This observation is similar to that for iGDGTs as discussed above (section 4.3.2), suggesting comparable ecology of the source organisms of OH-GDGTs and

375 iGDGTs if they are not even derived from identical organisms. This is likely attributed to favorable conditions for planktonic archaea in winter, although not clearly known, such as relatively high nutrient levels, low light, and high concentrations of SPM in the upper water due to the enhancement of vertical mixing driven by a combinantion of surface cooling and strong winter monsoon winds (Wong et al., 2015).

However, sedimentary RI-OH has been observed to be more significantly correlated with summer and autumn SSTs than

380 with SSTs from other seasons in the China coastal seas (CCSs), including the northern SCS studied here (Lü et al., 2015). We noted that the SCS is located at the warmest region of CCSs with the smallest seasonal and spatial SST amplitudes, as compared with the higher-latitude seas, e.g., the ECS. The response of RI-OH to SST in such an environment could be different from that for wider SST ranges in larger scale investigations. In other words, local investigations and calibrations are generally preferable for a specific study. Nevertheless, we admit that more studies on OH-GDGTs in various regions are

385 needed for a better assessment of the proxy.

5 Conclusions

Temperature estimates from $U_{37}^{K'}$, LDI, TEX_{86}^H and RI-OH proxies in surface sediments from the northern South China Sea shelf, including the Pearl River Estuary and the coastal area, were compared with annual and seasonal satellite-derived SST (WOA13). $U_{37}^{K'}$-SST was found to be spring-biased, likely due to the blooming of alkenone source-organisms in late spring,

390 when river runoff, as well as the abundant terrestrial nutrients, are highest. The results also showed that terrestrial inputs have an appreciable impact on LDI, TEX_{86}^H and RI-OH proxies and lead to cold-biased (LDI and TEX_{86}^H) or warm-biased (RI-OH) temperature relative to SSTs. After excluding from the data set the samples subject to terrestrial input, these indices

exhibited different seasonal variabilities, which reflect distinctive ecologies of their source organisms as results of seasonal changes in environmental conditions. LDI-SST matched well with annual SSTs, possibly related with the insensitivity of

395 marine eustigmatophytes to nutrient variations in an annual cycle. For the TEX_{86}^{H} proxy, a local "shallow water" calibration based on winter surface water SPM in the SCS appeared more appropriate for temperature reconstruction in this study and greatly reduced winter residuals. Similar to the TEX_{86}^{H}, RI-OH seems to reflect winter SST, and hence indicates comparable ecology of the source organisms of OH-GDGTs and iGDGTs if they are not identical. The winter biased TEX_{86}^{H} and RI-OH proxies can likely be attributed to favorable conditions for planktonic archaea in winter, impacted by the enhancement of

400 local vertical seawater mixing.

Acknowledgements

This work is supported by the National Natural Science Foundation of China (grant No. 41676030). BW thanks the China Scholarship Council (201706260033) for the support during his stay at Alfred Wegener Institute (Germany). We acknowledge the captain, crew and scientists who participated in the expeditions for collecting samples used in this study.

405 We appreciate the assistance from Jens Hefter for biomarker analysis at Alfred Wegener Institute.

Data availability

The data produced in this publication will be available from the PANGAEA database: https://doi.pangaea.de/10.1594/PANGAEA.905187.

Author contribution

410 GJ and GM conceived and designed the study. BW and MK collected the samples. BW conducted all the proxies analysis and was aid by JH in the instrument maintenance and data analysis. BW wrote the paper with inputs from GJ, GM and EP. All the authors reviewed the final manuscript.

Supplement

There is supplement related to this article.

415 **References**

Balzano, S., Lattaud, J., Villanueva, L., Rampen, S., Brussaard, C. P. D., van Bleijswijk, J., Bale, N., Sinninghe Damsté, J. S. and Schouten, S.: A quest for the biological sources of the ubiquitous long chain alkyl diols in the western tropical North

Atlantic Ocean, Biogeosciences, 5951–5968, doi:10.5194/bg-2018-97, 2018.

de Bar, M. W., Dorhout, D. J. C., Hopmans, E. C., Rampen, S. W., Sinninghe Damsté, J. S. and Schouten, S.: Constraints on

420   the application of long chain diol proxies in the Iberian Atlantic margin, Org. Geochem., 101, 184–195, doi:10.1016/j.orggeochem.2016.09.005, 2016.

Bijma, J., Altabet, M., Conte, M., Kinkel, H., Versteegh, G. J. M., Volkman, J. K., Wakeham, S. G. and Weaver, P. P.: Primary signal: Ecological and environmental factors-Report from Working Group 2, Geochemistry, Geophysics. Geosystems, 2(1), doi:10.1029/2000gc-000051, 2001.

425   Brassell, S. C., Eglinton, G., Marlowe, T., Phaumann, U.: Molecular stratigraphy: a new tool for climatic assessment, Nature, 320(6058): 129, 1986.

Chen, J., Hu, P., Li, X., Yang, Y., Song, J., Li, X., Yuan, H., Li, N. and Lü, X.: Impact of water depth on the distribution of iGDGTs in the surface sediments from the northern South China Sea: applicability of TEX$_{86}$ in marginal seas, Front. Earth Sci., 12(1), 95–107, doi:10.1007/s11707-016-0620-1, 2018.

430   Chen, Y., Zhang, C., Jia, C., Zheng, F. and Zhu, C.: Tracking the signals of living archaea: A multiple reaction monitoring (MRM) method for detection of trace amounts of intact polar lipids from the natural environment, Org. Geochem., 97, 1–4, doi:10.1016/j.orggeochem.2016.04.006, 2016.

Chen, Y. ling L., Chen, H. Y. and Chung, C. W.: Seasonal variability of coccolithophore abundance and assemblage in the northern South China Sea, Deep. Res. Part II Top. Stud. Oceanogr., 54(14–15), 1617–1633, doi:10.1016/j.dsr2.2007.05.005,

435   2007.

Conte, M. H., Sicre, M., Rühlemann, C., Weber, J. C., Schulte, S., Schulz-Bull, D. and Blanz, T.: Global temperature calibration of the alkenone unsaturation index ($U^{K'}_{37}$) in surface waters and comparison with surface sediments, Geochemistry, Geophys. Geosystems, 7(2), doi:10.1029/2005GC001054, 2006.

Dai, S. B., Yang, S. L. and Cai, A. M.: Impacts of dams on the sediment flux of the Pearl River, southern China, Catena,

440   76(1), 36–43, doi:10.1016/j.catena.2008.08.004, 2008.

Eglinton, T. I. and Eglinton, G.: Molecular proxies for paleoclimatology, Earth Planet. Sci. Lett., 275(1–2), 1–16, doi:10.1016/j.epsl.2008.07.012, 2008.

Farrimond, P., Eglinton, G. and Brassell, S. C.: Alkenones in Cretaceous black shales, Blake-Bahama Basin, western North Atlantic, Org. Geochem., 10(4–6), 897–903, doi:10.1016/S0146-6380(86)80027-4, 1986.

445   Ge, H., Zhang, C. L., Dang, H., Zhu, C. and Jia, G.: Distribution of tetraether lipids in surface sediments of the northern South China Sea: Implications for TEX$_{86}$ proxies, Geosci. Front., 4(2), 223–229, doi:10.1016/j.gsf.2012.10.002, 2013.

Ge, H., Zhang, C. L., Li, J., Versteegh, G. J. M., Hu, B., Zhao, J. and Dong, L.: Tetraether lipids from the southern Yellow Sea of China: Implications for the variability of East Asia Winter Monsoon in the Holocene, Org. Geochem., 70, 10–19, doi:10.1016/j.orggeochem.2014.02.011, 2014a.

450   Ge, Q., Liu, J. P., Xue, Z. and Chu, F.: Dispersal of the Zhujiang River (Pearl River) derived sediment in the Holocene, Acta Oceanol. Sin., 33(8), 1–9, doi:10.1007/s13131-014-0407-8, 2014b.

Häggi, C., Schefuß, E., Sawakuchi, A. O., Chiessi, C. M., Mulitza, S., Bertassoli Jr, D. J., Hefter, J., Zabel, M., Baker, P. A. and Schouten, S.: Modern and late Pleistocene particulate organic carbon transport by the Amazon River: Insights from long-chain alkyl diols, Geochim. Cosmochim. Acta, doi:10.1016/j.gca.2019.07.018, 2019.

455 Hopmans, E. C., Weijers, J. W. H., Schefuß, E., Herfort, L., Sinninghe Damsté, J. S. and Schouten, S.: A novel proxy for terrestrial organic matter in sediments based on branched and isoprenoid tetraether lipids, Earth Planet. Sci. Lett., 224(1–2), 107–116, doi:10.1016/j.epsl.2004.05.012, 2004.

Huguet, C., Fietz, S. and Rosell-Melé, A.: Global distribution patterns of hydroxy glycerol dialkyl glycerol tetraethers, Org. Geochem., 57, 107–118, doi:10.1016/j.orggeochem.2013.01.010, 2013.

460 Jia, G., Zhang, J., Chen, J., Peng, P. and Zhang, C. L.: Archaeal tetraether lipids record subsurface water temperature in the South China Sea, Org. Geochem., 50, 68–77, doi:10.1016/j.orggeochem.2012.07.002, 2012.

Jia, G., Wang, X., Guo, W. and Dong, L.: Seasonal distribution of archaeal lipids in surface water and its constraint on their sources and the TEX_{86} temperature proxy in sediments of the South China Sea, J. Geophys. Res. Biogeosciences, 122(3), 592–606, doi:10.1002/2016JG003732, 2017.

465 Kang, S., Shin, K. H. and Kim, J. H.: Occurrence and distribution of hydroxylated isoprenoid glycerol dialkyl glycerol tetraethers (OH-GDGTs) in the Han River system, South Korea, Acta Geochim., 36(3), 367–369, doi:10.1007/s11631-017-0165-3, 2017.

Kim, J. H., van der Meer, J., Schouten, S., Helmke, P., Willmott, V., Sangiorgi, F., Koç, N., Hopmans, E. C. and Damsté, J. S. S.: New indices and calibrations derived from the distribution of crenarchaeal isoprenoid tetraether lipids: Implications for 470 past sea surface temperature reconstructions, Geochim. Cosmochim. Acta, 74(16), 4639–4654, doi:10.1016/j.gca.2010.05.027, 2010.

Kim, J. H., Schouten, S., Rodrigo-Gámiz, M., Rampen, S., Marino, G., Huguet, C., Helmke, P., Buscail, R., Hopmans, E. C., Pross, J., Sangiorgi, F., Middelburg, J. B. M. and Sinninghe Damsté, J. S.: Influence of deep-water derived isoprenoid tetraether lipids on the TEX_{86}^{H} paleothermometer in the Mediterranean Sea, Geochim. Cosmochim. Acta, 150, 125–141, 475 doi:10.1016/j.gca.2014.11.017, 2015.

Kim, J. H., Villanueva, L., Zell, C. and Sinninghe Damsté, J. S.: Biological source and provenance of deep-water derived isoprenoid tetraether lipids along the Portuguese continental margin, Geochim. Cosmochim. Acta, 172, 177–204, doi:10.1016/j.gca.2015.09.010, 2016.

Lattaud, J., Kim, J. H., De Jonge, C., Zell, C., Sinninghe Damsté, J. S. and Schouten, S.: The C_{32} alkane-1,15-diol as a tracer 480 for riverine input in coastal seas, Geochim. Cosmochim. Acta, 202(12), 146–158, doi:10.1016/j.gca.2016.12.030, 2017.

Lincoln, S. A., Wai, B., Eppley, J. M., Church, M. J., Summons, R. E. and DeLong, E. F.: Planktonic Euryarchaeota are a significant source of archaeal tetraether lipids in the ocean, Proc. Natl. Acad. Sci., 111(27), 9858–9863, doi:10.1073/pnas.1409439111, 2014.

Liu, W., Zhang, C. L., Wang, Z., Wang, J., Liu, Z. and Don, H.: Distribution of glycerol dialkyl glycerol tetraethers in surface 485 sediments of Lake Qinghai and surrounding soil, Org. Geochem., 47, 78–87, doi:10.1016/j.orggeochem.2012.03.008, 2012a.

Liu, W. T. and Xie, X.: Space-based observations of the seasonal changes of South Asian monsoons and oceanic responses, Geophys. Res. Lett., 26(10), 1473–1476, doi:10.1029/1999GL900289, 1999.

Liu, X. L., Lipp, J. S., Simpson, J. H., Lin, Y. S., Summons, R. E. and Hinrichs, K. U.: Mono- and dihydroxyl glycerol dibiphytanyl glycerol tetraethers in marine sediments: Identification of both core and intact polar lipid forms, Geochim.
490   Cosmochim. Acta, 89, 102–115, doi:10.1016/j.gca.2012.04.053, 2012b.

Liu, Y., Gao, S., Wang, Y. P., Yang, Y., Long, J., Zhang, Y. and Wu, X.: Distal mud deposits associated with the Pearl River over the northwestern continental shelf of the South China Sea, Mar. Geol., 347, 43–57, doi:10.1016/j.margeo.2013.10.012, 2014.

Lopes Dos Santos, R. A., Spooner, M. I., Barrows, T. T., De Deckker, P., Sinninghe Damsté, J. S. and Schouten, S.:
495   Comparison of organic ($U_{37}^{K'}$, TEX_{86}^{H}, LDI) and faunal proxies (foraminiferal assemblages) for reconstruction of late Quaternary sea surface temperature variability from offshore southeastern Australia, Paleoceanography, 28(3), 377–387, doi:10.1002/palo.20035, 2013.

Lü, X., Yang, H., Song, J., Versteegh, G. J. M., Li, X., Yuan, H., Li, N., Yang, C., Yang, Y., Ding, W. and Xie, S.: Sources and distribution of isoprenoid glycerol dialkyl glycerol tetraethers (GDGTs) in sediments from the east coastal sea of China:
500   Application of GDGT-based paleothermometry to a shallow marginal sea, Org. Geochem., 75, 24–35, doi:10.1016/j.orggeochem.2014.06.007, 2014.

Lü, X., Liu, X. L., Elling, F. J., Yang, H., Xie, S., Song, J., Li, X., Yuan, H., Li, N. and Hinrichs, K. U.: Hydroxylated isoprenoid GDGTs in Chinese coastal seas and their potential as a paleotemperature proxy for mid-to-low latitude marginal seas, Org. Geochem., 89–90, 31–43, doi:10.1016/j.orggeochem.2015.10.004, 2015.

505   Lü, X., Chen, J., Han, T., Yang, H., Wu, W., Ding, W. and Hinrichs, K. U.: Origin of hydroxyl GDGTs and regular isoprenoid GDGTs in suspended particulate matter of Yangtze River Estuary, Org. Geochem., 128, 78–85, doi:10.1016/j.orggeochem.2018.12.010, 2019.

Lu, Z. and Gan, J.: Controls of seasonal variability of phytoplankton blooms in the Pearl River Estuary, Deep. Res. Part II Top. Stud. Oceanogr., 117, 86–96, doi:10.1016/ j.dsr2.2013.12.011, 2015.

510   Müller, P. J., Kirst, G., Ruhland, G., Von Storch, I. and Rosell-Melé, A.: Calibration of the alkenone paleotemperature index $U_{37}^{K'}$ based on core-tops from the eastern South Atlantic and the global ocean (60° N–60° S), Geochim. Cosmochim. Acta, 62(10), 1757–1772, 10.1016/S0016-7037(98)00097-0, 1998.

Paasche, E.: A review of the coccolithophorid Emiliania huxleyi (Prymnesiophyceae), with particular reference to growth, coccolith formation, and calcification-photosynthesis interactions, Phycologia, 40(6), 503–529, doi:10.2216/i0031-8884-40-
515   6-503.1, 2010.

Park, E., Hefter, J., Fischer, G., Hvitfeldt Iversen, M., Ramondenc, S., Nthig, E. M. and Mollenhauer, G.: Seasonality of archaeal lipid flux and GDGT-based thermometry in sinking particles of high-latitude oceans: Fram Strait (79° N) and Antarctic Polar Front (50° S), Biogeosciences, 16(11), 2247–2268, doi:10.5194/bg-16-2247-2019, 2019.

Prahl, F. G. and Wakeham, S. G.: Calibration of unsaturation patterns in long-chain ketone compositions for

520 palaeotemperature assessment, Nature, 330(6146), 367, 1987.

Rampen, S. W., Schouten, S. and Wakeham, S. G.: Seasonal and spatial variation in the sources and fluxes of long chain diols and mid-chain hydroxy methyl alkanoates in the Arabian Sea, , 38, 165–179, doi:10.1016/j.orggeochem.2006.10.008, 2007.

Rampen, S. W., Willmott, V., Kim, J. H., Uliana, E., Mollenhauer, G., Schefuß, E., Sinninghe Damsté, J. S. and Schouten, S.:

525 Long chain 1,13- and 1,15-diols as a potential proxy for palaeotemperature reconstruction, Geochim. Cosmochim. Acta, 84, 204–216, doi:10.1016/j.gca.2012.01.024, 2012.

Rampen, S. W., Willmott, V., Kim, J., Rodrigo-gámiz, M., Uliana, E., Mollenhauer, G., Schefuß, E., Sinninghe, J. S. and Schouten, S.: Organic Geochemistry Evaluation of long chain 1,14-alkyl diols in marine sediments as indicators for upwelling and temperature, Org. Geochem., 76, 39–47, doi:10.1016/j.orggeochem.2014.07.012, 2014a.

530 Rampen, S. W., Datema, M., Rodrigo-Gamiz, M., Schouten, S., Reichart, G. and Damste, J. S. S.: Sources and proxy potential of long chain alkyl diols in lacustrine environments, Geochim. Cosmochim. Acta,144, 59–71, doi:10.1016/j.gca.2014.08.033, 2014b.

Rosell-Melé, A. and Prahl, F. G.: Seasonality of $U_{37}^{K'}$ temperature estimates as inferred from sediment trap data, Quat. Sci. Rev., 72, 128–136, doi:10.1016/j.quascirev.2013.04.017, 2013.

535 Schouten, S., Hopmans, E. C., Schefuß, E. and Sinninghe Damsté, J. S.: Distributional variations in marine crenarchaeotal membrane lipids: a new tool for reconstructing ancient sea water temperatures? Earth Planet. Sci. Lett., 204(1–2), 265–274, 2002.

Schouten, S., Hopmans, E. C. and Sinninghe Damsté, J. S.: The organic geochemistry of glycerol dialkyl glycerol tetraether lipids: A review, Org. Geochem., 54, 19–61, doi:10.1016/j.orggeochem.2012.09.006, 2013.

540 Sinninghe Damsté, J. S., Rijpstra, W. I. C., Hopmans, E. C., Jung, M. Y., Kim, J. G., Rhee, S. K., Stieglmeier, M. and Schleper, C.: Intact polar and core glycerol dibiphytanyl glycerol tetraether lipids of group I.1a and I.1b Thaumarchaeota in soil, Appl. Environ. Microbiol., 78(19), 6866–6874, doi:10.1128/AEM.01681-12, 2012.

Smith, M., Deckker, P. De, Rogers, J., Brocks, J., Hope, J., Schmidt, S., Lopes, R. and Schouten, S.: Comparison of $U_{37}^{K'}$, TEX_{86}^{H} and LDI temperature proxies for reconstruction of south-east Australian ocean temperatures, Org. Geochem., 64, 94–

545 104, doi:10.1016/j.org-geochem.2013.08.015, 2013.

Su, J.: Overview of the South China Sea circulation and its influence on the coastal physical oceanography outside the Pearl River Estuary, Cont. Shelf Res., 24(16), 1745–1760, doi:10.1016/j.csr.2004.06.005, 2004.

Tierney, J. E. and Tingley, M. P.: BAYSPLINE: A New Calibration for the Alkenone Paleothermometer, Paleoceanogr. Paleoclimatology, 33(3), 281–301, doi:10.1002/2017PA-003201, 2018.

550 Turich, C., Freeman, K. H., Bruns, M. A., Conte, M., Jones, A. D. and Wakeham, S. G.: Lipids of marine Archaea: Patterns and provenance in the water-column and sediments, Geochim. Cosmochim. Acta, 71(13), 3272–3291, doi:10.1016/j.gca.2007.04.013, 2007.

Versteegh, G. J. M. and Leeuw, J. W. D. E.: Potential palaeoenvironmental information of C_{24} to C_{36} mid-chain diols, keto-

ols and mid-chain hydroxy fatty acids; a critical review, Org. Geochem., 27(97), 1–13, https://doi.org/10.1016/S0146-
555 6380(97)00063-6, 1997.

Volkman J. K., Barrett, S. M., Blackburn S. I., Sikes, E. L.: Alkenones in *Gephyrocapsa oceanica*: Implications for studies
of paleoclimate, Geochim. Cosmochim. Acta, 59(3), 513–520, doi:10.1016/0016-7037(95)00325-T, 1995.

Volkman, J. K., Barrett, S. M., Blackburn, S. I.: Eustigmatophyte microalgae are potential sources of C_{29} sterols, C_{22}–C_{28} n-
alcohols   and C_{28}–C_{32} n-alkyl   diols   in   freshwater   environments,   Org.   Geochem.,   30(5):   307–318,
560 doi:10.1016/S01466380(99)00009-1, 1999.

Wang, J. X., Wei, Y., Wang, P., Hong, Y. and Zhang, C. L.: Unusually low TEX_{86} values in the transitional zone between
Pearl River estuary and coastal South China Sea: Impact of changing archaeal community composition, Chem. Geol., 402,
18–29, doi:10.1016/j.chem-geo.2015.03.002, 2015.

Wei, Y., Wang, J., Liu, J., Dong, L., Li, L., Wang, H., Wang, P., Zhao, M. and Zhang, C. L.: Spatial variations in archaeal
565 lipids of surface water and core-top sediments in the South China Sea and their implications for paleoclimate studies, Appl.
Environ. Microbiol., 77(21), 7479–7489, doi:10.1128/AEM.00580-11, 2011.

Weijers, J. W. H., Schouten, S., Spaargaren, O. C. and Sinninghe Damsté, J. S.: Occurrence and distribution of tetraether
membrane lipids in soils: Implications for the use of the TEX_{86} proxy and the BIT index, Org. Geochem., 37(12), 1680–
1693, doi:10.1016/j.orggeochem.-2006.07.018, 2006.

570 Weijers, J. W. H., Lim, K. L. H., Aquilina, A., Damsté, J. S. S. and Pancost, R. D.: Biogeochemical controls on glycerol
dialkyl glycerol tetraether lipid distributions in sediments characterized by diffusive methane flux, Geochemistry, Geophys.
Geosystems, 12(10), 1–15, doi:10.1029/2011GC003724, 2011.

Wong, G. T. F., Pan, X., Li, K. Y., Shiah, F. K., Ho, T. Y. and Guo, X.: Hydrography and nutrient dynamics in the Northern
South China Sea Shelf-sea (NoSoCS), Deep. Res. Part II: Top. Stud. Oceanogr., 117, 23–40, doi:10.1016/j.dsr2.2015.02.023,
575 2015.

Xie, W., Zhang, C., Zhou, X. and Wang, P.: Salinity-dominated change in community structure and ecological function of
Archaea from the lower Pearl River to coastal South China Sea, Appl. Microbiol. Biotechnol., 98(18), 7971–7982,
doi:10.1007/s00253-014-5838-9, 2014.

Xu, J., Yin, K., He, L., Yuan, X., Ho, A. Y. T. and Harrison, P. J.: Phosphorus limitation in the northern South China Sea
580 during late summer: Influence of the Pearl River, Deep. Res. Part I: Oceanogr. Res. Pap., 55(10), 1330–1342,
doi:10.1016/j.dsr.2008.05.007, 2008.

Yang, Y., Gao, C., Dang, X., Ruan, X., Lü, X., Xie, S., Li, X., Yao, Y. and Yang, H.: Assessing hydroxylated isoprenoid
GDGTs   as   a   paleothermometer   for   the   tropical   South   China   Sea,   Org.   Geochem.,   115,   156–165,
doi:10.1016/j.orggeochem.2017.10.014, 2018.

585 Zhang, C. L., Wang, J., Wei, Y., Zhu, C., Huang, L. and Dong, H.: Production of branched tetraether lipids in the lower Pearl
River and estuary: Effects of extraction methods and impact on bGDGT proxies, Front. Microbiol., 2(JAN), 1–18,
doi:10.3389/fmicb.2011.00274, 2012.

Zhang, J., Bai, Y., Xu, S., Lei, F. and Jia, G.: Alkenone and tetraether lipids reflect different seasonal seawater temperatures in the coastal northern South China Sea, Org. Geochem., 58, 115–120, doi:10.1016/j.orggeochem.2013.02.012, 2013.

590 Zhang, J., Jia, G., Guo, W., Wang, X. and Lei, F.: Isoprenoid tetraether lipids in suspended particulate matter from the East China Sea and implication for sedimentary records, Org. Geochem., 114, 81–90, doi:10.1016/j.orggeochem.2017.09.006, 2017.

Zhang, Y. G., Pagani, M. and Wang, Z.: Ring Index: A new strategy to evaluate the integrity of TEX86 paleothermometry, Paleoceanography, 31(2), 220–232, doi:10.1002/2015PA002848, 2016.

595 Zhou, H., Hu, J., Spiro, B., Peng, P. and Tang, J.: Glycerol dialkyl glycerol tetraethers in surficial coastal and open marine sediments around China: Indicators of sea surface temperature and effects of their sources, Palaeogeogr. Palaeoclimatol. Palaeoecol., 395, 114–121, doi:10.1016/j.palaeo.2013.12.006, 2014.

Zhu, X., Mao, S., Wu, N., Sun, Y. and Guan, H.: Molecular and stable carbon isotopic compositions of saturated fatty acids within one sedimentary profile in the Shenhu, northern South China Sea: Source implications, J. Asian Earth Sci., 92, 262–
600 275, doi:10.1016/j.jseaes.2013.12.011, 2014.

Zhu, X., Jia, G., Mao, S. and Yan, W.: Sediment records of long chain alkyl diols in an upwelling area of the coastal northern South China Sea, Org. Geochem., 121, 1–9, doi:10.1016/j.orggeochem.2018.03.014, 2018.

Table 1: Pearson correlation analysis of different diols in surface sediments in this study.

Pearson correlation coefficient	C_{28} 1,13-diol	C_{30} 1,13-diol	C_{30} 1,15-diol	C_{32} 1,15-diol
C_{28} **1,13-diol**	1			
C_{30} **1,13-diol**	0.83**	1		
C_{30} **1,15-diol**	−0.68**	−0.90**	1	
C_{32} **1,15-diol**	0.56**	0.78**	−0.90**	1

605 **** P-value < 0.005**
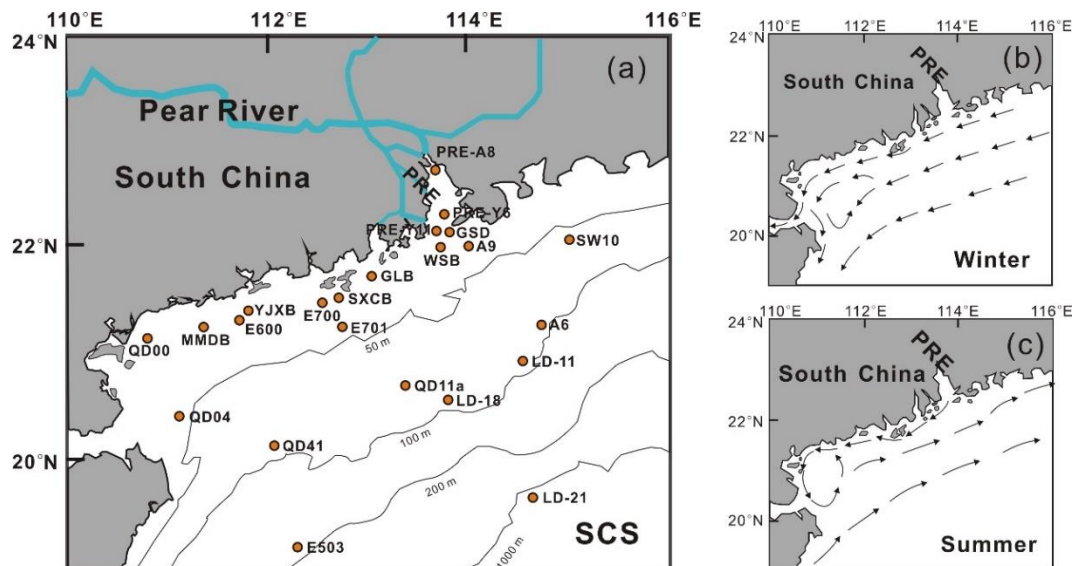
Figure 1: (a) Sampling sites and patterns of the surface coastal currents in (b) winter and (c) summer, respectively (modified from Liu et al. (2014)).
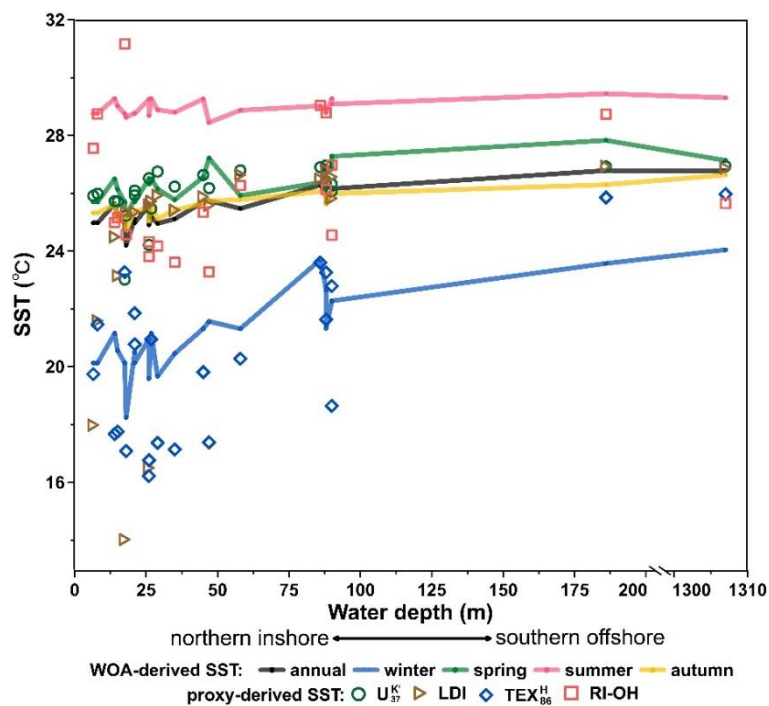
610   **Figure 2: Changes with water depth of WOA-derived and proxy-derived SSTs.**
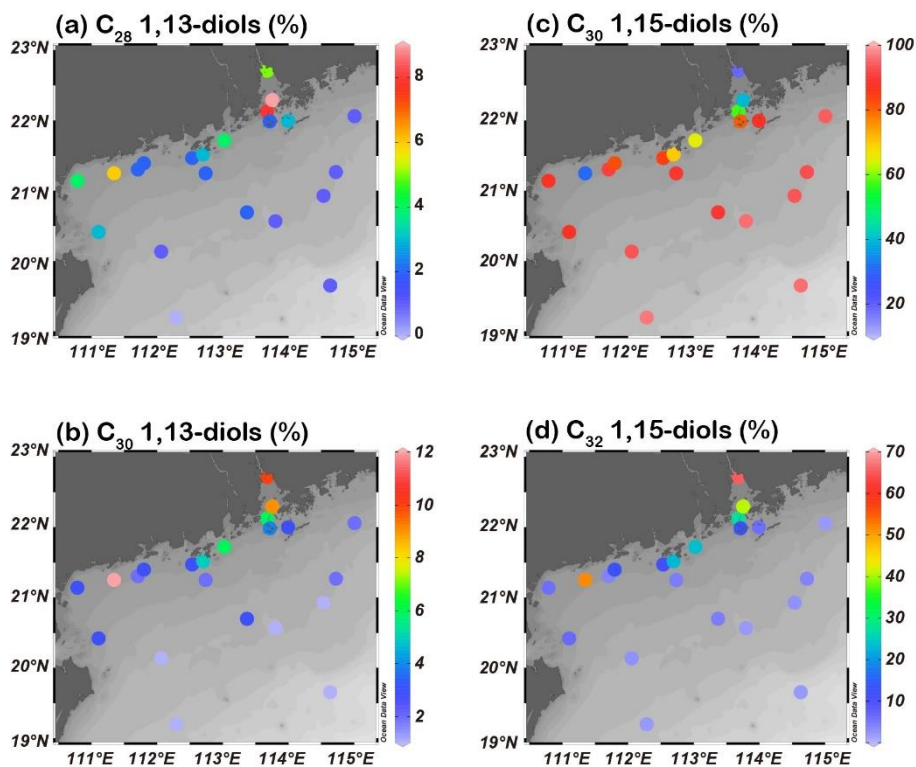
Figure 3: Distribution of relative abundances of: (a) C$_{28}$ 1,13-diol, (b) C$_{30}$ 1,13-diol, (c) C$_{30}$ 1,15-diol, and (d) C$_{32}$ 1,15-diol.
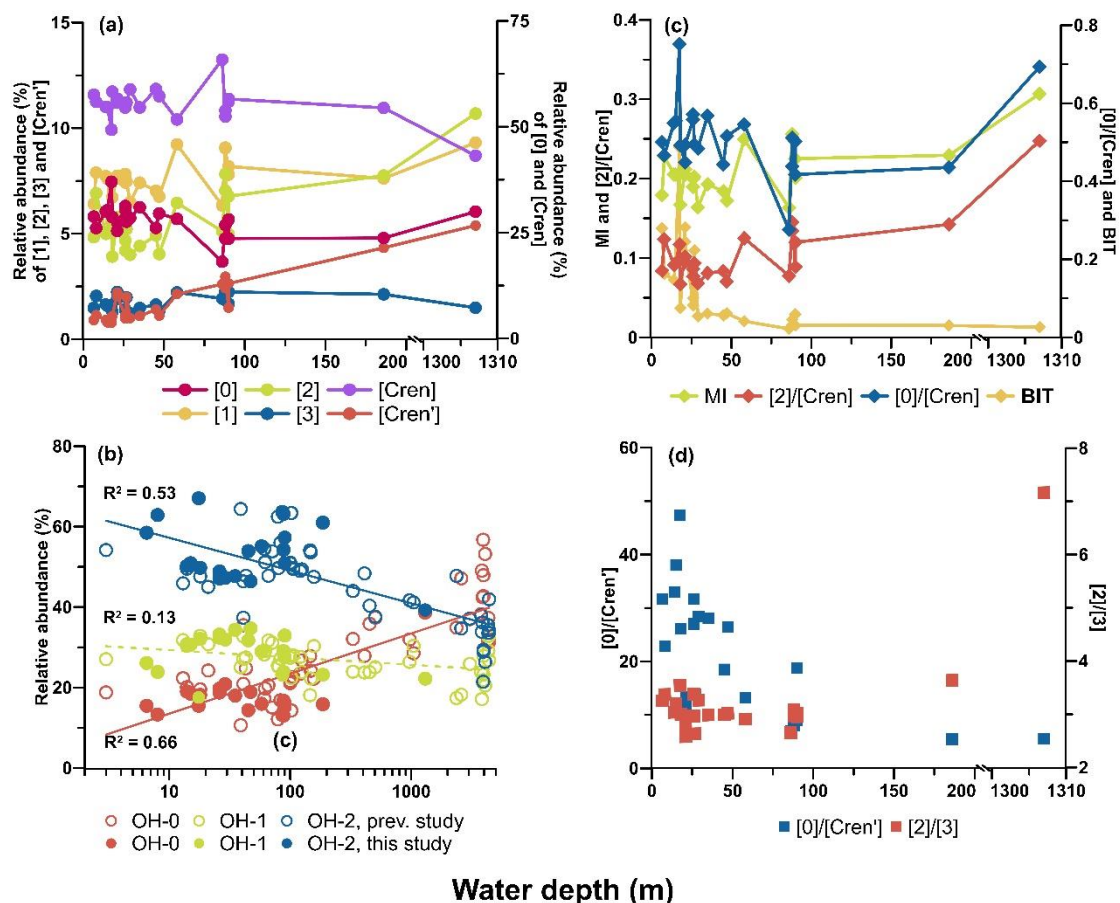
Figure 4: Depth profiles of (a) the relative abundance of individual iGDGTs, (b) the relative abundance of individual OH-GDGTs (open dots represent data from Lü et al., 2015 and Yang et al., 2018, and solid dots represent data from this study), (c) MI and BIT index values, as well as [0]/[Cren] and [2]/[Cren] ratios, and (d) [0]/[Cren'] and [2]/[3] ratios.
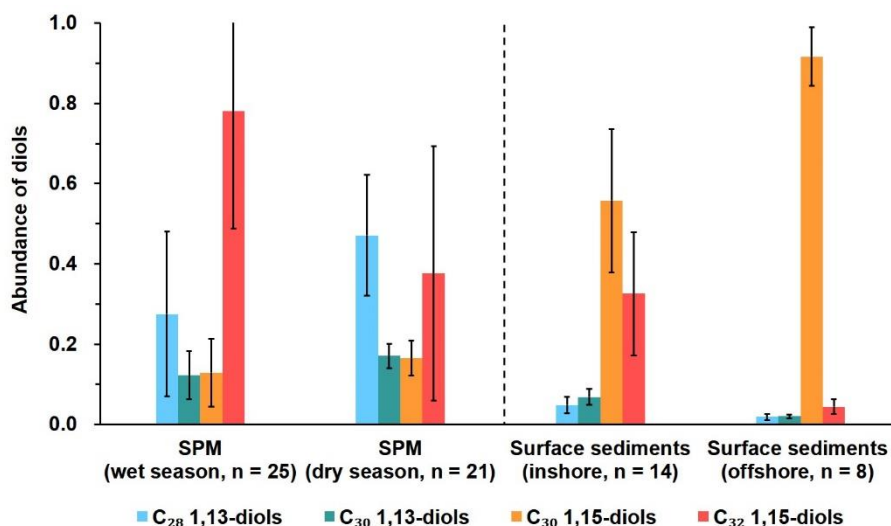
Figure 5: Average diol distributions in SPM in the PRE (data from Zhu et al. (2018)), inshore and offshore surface sediments (data from this study) (Error bars indicate the standard deviations).
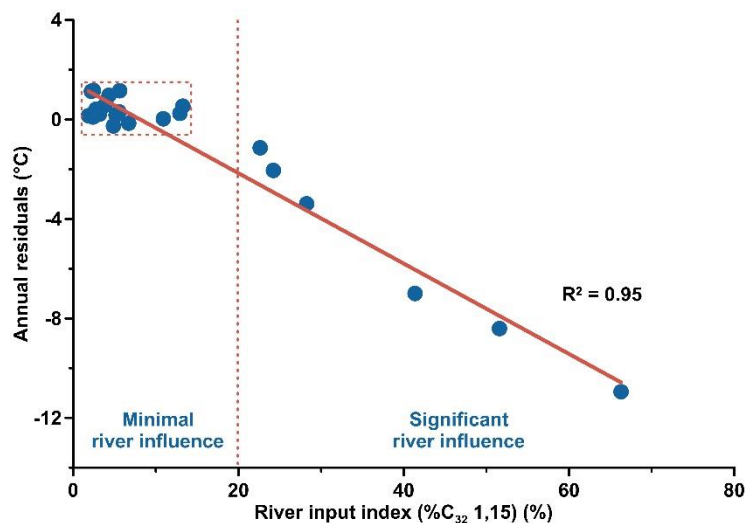
620

Figure 6: Annual SST residuals with %C_{32} 1,15 diol suggestive of river input.
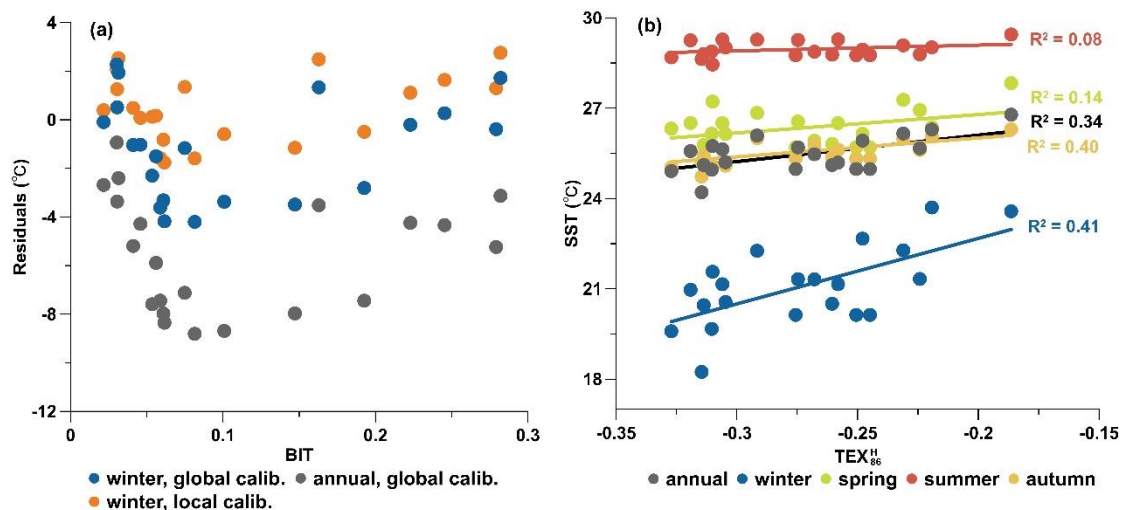
Figure 7: (a) Residual changes with BIT values of the annual and winter estimates based on the global calibration (Kim et al., 2010) and winter residuals based on the local calibration from winter SPM (Jia et al., 2017), and (b) relationships of TEX_{86}^{H} with annual and seasonal SSTs.

625
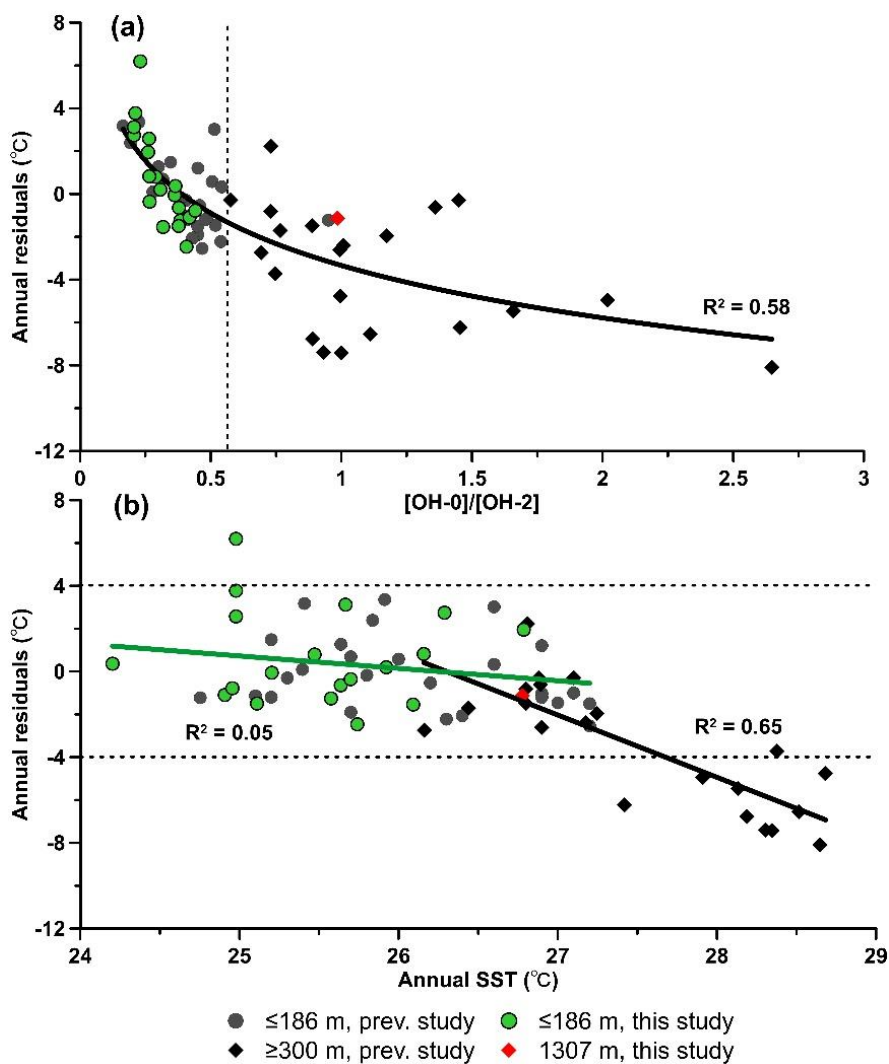
Figure 8: Changes of annual residuals with (a) [OH-0]/[OH-2] ratios (solid line is a fitting line), and (b) annual SST (green and black solid lines are fitting lines for "shallow water" and "deep water" samples, respectively).
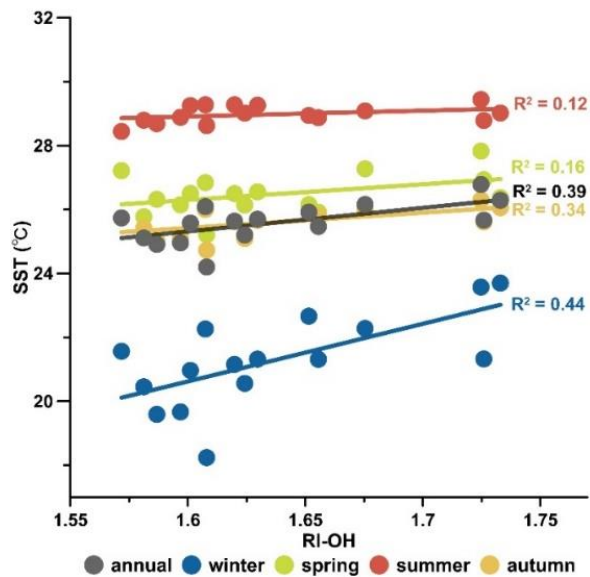
Figure 9: Correlation plots of RI-OH with annual and seasonal SST (solid lines are linear fitting lines).